JAAS

ROYAL SOCIETY OF CHEMISTRY

TECHNICAL NOTE

View Article Online
View Journal | View Issue

Cite this: *J. Anal. At. Spectrom.*, 2025, **40**, 2649

Single particle ICP-TOFMS for the detection of micro-scale polystyrene and polyvinyl chloride from artificially aged bulk plastic

Raquel Gonzalez de Vega, [a] Maximilian J. Huber,[b] Isabel S. Jüngling,[b] Natalia P. Ivleva [b] and David Clases *[c]

A method for the simultaneous analysis of carbon (C) and chlorine (Cl) in individual microplastic particles (MPs) using single particle (SP) inductively coupled plasma – time-of-flight mass spectrometry (ICP-TOFMS) was developed. The approach exploited hydrogen-assisted cluster ion formation to monitor Cl as $^{35}ClH_2^+$ and was applied in conjunction with a collision/reaction cell that used an altered radiofrequency amplitude to balance ion transmission for both C^+ and ClH_2^+. This strategy improved detection limits for Cl-bearing particles and enabled co-detection of C and Cl within the same SP event. As a proof of concept, artificially aged polystyrene (PS) and polyvinyl chloride (PVC) were analysed. Discrimination of MP polymers was achieved by detecting either only C in a SP event (PS) or the coincident detection of C and Cl (PVC). Critical detection thresholds of 1.2 μm (0.8 pg, *via* C) for PS and 1.4 μm (0.8 pg, *via* C) or 1.3 μm (0.9 pg, *via* Cl) for PVC were determined. Particles larger than ~10 μm, however, were poorly transported by the nebulisation system, limiting effective detection to smaller MPs.

Received 30th May 2025
Accepted 8th September 2025

DOI: 10.1039/d5ja00213c

rsc.li/jaas

Introduction

Microplastic (MP) particles in the size range of 1 μm to 5 mm,[1,2] have become a major environmental concern. They originate from diverse polymers and are primarily generated through the aging and degradation of bulk plastics driven by photo-degradation, mechanical abrasion, and biological activity. Once released into aquatic ecosystems, MPs are highly persistent, mobile, and capable of interacting with biota, thereby posing long-term risks to environmental health and biodiversity.[3,4] The resulting secondary MPs exhibit a wide range of sizes, shapes, and chemical compositions, and their small size makes them increasingly elusive, presenting significant analytical challenges in complex environmental matrices.[5]

Conventional analytical techniques for microplastic analysis, such as Fourier-transform infrared spectroscopy (FTIR), Raman spectroscopy, thermal analysis, and microscopic methods such as light and scanning electron microscopy (SEM), may provide valuable insights into polymer composition, particle morphology and/or sizes.[6] However, these methods are often labour-intensive and are prone to artefacts during sample preparation and often impacted by complex sample matrices. As such, they are limited in their capability to pinpoint MPs among a large colloidal background, to characterise sufficient numbers of particles and to provide in-depth characterisations of small particles.[1] An increasingly important avenue to detect and characterise MPs is mass spectrometry (MS), which offers highly selective and sensitive methods. Especially new approaches in elemental mass spectrometry have opened new possibilities for the analysis of small MP below 20 μm.[7] Inductively coupled plasma-mass spectrometry (ICP-MS) in its single particle (SP) mode has emerged as an interesting tool to detect and characterise individiual MPs. Carbon remains the most obvious target for MP characterisation and strategies are increasingly directed to detect either the ^{12}C or ^{13}C isotope.[8–10] However, heteroelements such as chlorine (Cl) and fluorine (F) provide further opportunities to detect and characterise MPs. For instance, the detection of Cl is particularly useful to study polyvinyl chloride (PVC) MPs,[7] while F analysis offers access to fluoropolymers.[11–13]

ICP-MS employing a time-of-flight mass analyser (ICP-TOFMS) has provided new capabilities to characterise particles. Unlike quadrupole-based instruments, it enables the detection of various elements/isotopes within the same particle thereby contributing to a more comprehensive understanding of composition, mixing states and enabling new ways for non-target screenings.[14,15] The ability to capture multi-elemental data in a single analysis significantly improves the capability to characterise particles and as such, SP ICP-TOFMS shows promise as tool for MP investigations and has recently been employed by some groups.[7,16–18] The ability to simultaneously target carbon alongside plastic-associated heteroelements can

[a]*TESLA-Analytical Chemistry, Institute of Chemistry, University of Graz, Graz, Austria*
[b]*Chair of Analytical Chemistry and Water Chemistry, Institute of Water Chemistry, Technical University of Munich, Garching, Germany*
[c]*NanoMicroLab, Institute of Chemistry, University of Graz, Graz, Austria. E-mail: david.clases@uni-graz.at*

be useful to differentiate MP polymers and may provide information on adsorbed contaminants such as heavy metals opening new avenues for more comprehensive characterisations. However, in some cases, in which matrices are too complex, and a plethora of different particulate C-sources may be present, more selective methods are required.[18] Nonetheless, in cases where MP species can be discriminated based on the presence of heteroatoms, SP ICP-TOFMS provides facile options to carry out controlled experiments (*e.g.*, degradation experiments[13]).

This study explores the application of SP ICP-TOFMS for the detection and characterisation of secondary microplastics (MPs) generated from artificially aged bulk polymers. As a proof of concept, we analysed polystyrene (PS) and polyvinyl chloride (PVC) together, showing that particles can be distinguished by the sole detection of C (PS) or by the co-detection of C and Cl (PVC). While this binary case illustrates the capability of the method, the broader innovation lies in the development of an optimised SP ICP-TOFMS workflow for reliable detection of low-mass elements. Specifically, the use of hydrogen-assisted ClH_2^+ cluster ion detection, combined with RF optimisation of the collision/reaction cell, enabled balanced transmission of C and Cl and improved detection limits for Cl-bearing particles. However, the limits and implications for quantitative analysis are discussed critically in this work.

Materials and methods

Chemicals

Polystyrene microplastic (MP) standards with diameters of 4 μm and 5 μm were obtained from Sigma-Aldrich (St. Louis, MO, USA). Prior to analysis, the stock solutions were briefly sonicated and diluted in polypropylene containers for SP ICP-TOFMS measurements. Ultra-pure water in the same containers was handled accordingly and analysed as blank to ensure the absence of polypropylene MPs. An elemental Cl standard at a concentration of 1000 mg ml^{-1} (Single-Element ICP Standard-Solution Roti®Star, Carl Roth®, Karlsruhe, Germany) and a carbon solution prepared from sodium carbonate (Na_2CO_3 ≥ 99,5%, p.a., ACS, anhydrous, Carl Roth®) were diluted to working concentrations using ultrapure water (18.2 MΩ cm, Merck Millipore, Bedford, USA). While previous studies used organic C standards for the estimation of the C response, Na_2CO_3 was chosen in this study as it showed low volatility and consistent responses across longer time scales.

Artificially aged bulk plastic

Secondary microplastics of PS and PVC were generated according to a protocol by von der Esch *et al.*[19] with some modifications mentioned below. Square pieces (approx. 1 mm × 1 cm × 1 cm) of both plastic polymers (each individually and combined) were treated in an ultrasonication bath (35 kHz, SONOREX SUPER RK 514 Ultra sonic bath, BANDELIN electronic GmbH & Co. KG, Germany) for 32 h in 15 ml ultrapure water (Milli-Q Integral 5, Merck Millipore, Germany, resistance 18.2 M Ω cm). Secondary MPs were produced in three batches and subsequently combined.

Sample preparation

Raman microscopy and SEM-EDX analysis were used to investigate secondary plastics and to provide tentative insights into mean sizes. Here, sample aliquots were prepared in a laminar flow bench (ENVAIR eco air V, CARLO ERBA Reagents GmbH, Germany) to minimise particle contamination. Using an overhead stirrer (350 min^{-1}, RZR 2000, Heidolph Instruments GmbH & Co. KG, Germany) and a flow breaker construction according to Wolff *et al.*[20], a 20 ml (10 ml for mixed sample) aliquots were taken after diluting 1.5 ml of sample in 400 ml ultrapure water. Subsequently each aliquot was filtered with a Si-filter (10 mm × 10 mm, 1 μm pore size, SmartMembranes GmbH, Germany) and rinsed with 30 ml ultrapure water and 30 ml ethanol (puriss. p.a., absolute, ≥ 99.8% (GC), Sigma-Aldrich, Germany). All chemicals used for sample preparation and filtration were additionally filtered through a 0.22 μm polyvinylidene fluoride (PVDF) filter membrane (Durapore, hydrophilic, nonsterile, Merck, Germany). The filter system consisted of a 500 ml holding flask, a custom-made PVDF filter support, two soft silicone gaskets, and a 100 ml glass filter funnel. Samples were concentrated onto a circular area with a diameter of approximately 6 mm, and a laboratory blank was prepared following the same procedure. The use of 1 μm pore size Si filters introduced a lower size cut-off, excluding particles smaller than 1 μm from Raman and SEM-EDX analysis; however, this cut-off still enabled the analysis of small MPs within a similar size window to that analysable by SP ICP-TOFMS. For SP ICP-TOFMS measurements, secondary microplastic suspensions were sonicated for 10 s prior to analysis and agitated during aspiration to minimise sedimentation of larger MPs. For method optimisation, samples were diluted 1 : 5, while for the final analysis they were examined without dilution.

Raman microspectroscopy

Image acquisition and Raman measurements were performed using a WITec alpha300R (Oxford Instruments, United Kingdom) in combination with a 100× objective (EC Epiplan-Neofluar, N.A. = 0.9, Carl Zeiss Microscopy GmbH, Germany). A 532 nm DPSS laser was used at 20 mW with 20 accumulations of 0.1 s integration time. To control the instrument and perform automated image analysis, WITec Control SIX 6.2 and the in-house developed software TUM-ParticleTyper 2 (ref. 21) were used. Random Window Sampling was applied as a method. This method sets measurement windows of a given size randomly on the analysed filter surface and quantifies and measures the found particles. A filter radius of 3250 μm was considered for the analysis to ensure inclusion of border particles. The window size was 180 μm by 180 μm, of which a measurement field of 160 μm by 160 μm was set to ensure all measured particles were fully in the taken image. Only particles with a maximum Feret diameter between 1–20 μm were analysed. This window reflected approximately the size range detectable in SP ICP-MS.[7] To ensure a representative analysis, at least 20% of the total

filter area was considered. The spectra were analysed with the WITec TrueMatch/ParticleScout 6.2 application taking into consideration the spectral background of the Si-filter.

SEM-EDX analysis

The same filters used for the Raman measurements were also analysed with a Sigma 300 VP Field Emission SEM (FE-SEM, Carl Zeiss AG, Germany) in combination with an EDX detector (Quantax XFlash 6l60, Bruker Nano GmbH, Germany). An acceleration voltage of 10 kV, a working distance of around 8.5 mm and a magnification of 700 were employed for image acquisition with a BSE detector. The software Bruker ESPRIT 2.5 was used for particle recognition (feature mode) and EDX measurements.

SP ICP-TOFMS

A Vitesse ICP-TOFMS platform by Nu Instruments (Wrexham, UK) was operated in single particle mode. The plasma was maintained at 1300 W and He and H_2 were used as cell gasses and optimised for the joint analysis of Cl and C as described later. A MicroMist nebuliser coupled to a cyclonic spray chamber was used for sample introduction, with a typical nebuliser gas flow rate of approximately 1.1 L min^{-1}. The monitored masses ranged from 7 to 40 amu. The restriction of the mass range enabled increased sensitivity *via* "over pulsing" as discussed by Lockwood *et al.*.[22] Two spectra were binned before baseline correction and four after, with spectra stored every 90 μs. Data acquisition was conducted using Nu Codaq software (Nu Instruments) and data analysis was performed with the open-source python-based data processing platform "SPCal".[15,23] Compound Poisson statistics were applied to differentiate ionic background and noise from SP events with an α value of 10^{-6}. This threshold was simulated using a lognormal approximation as discussed in a previous study.[14,22,23]

For mass and size calibrations, ionic responses for C and Cl were determined using a series of ionic chloride and carbonate standards with ultra-pure water used for background subtraction. Subsequently, two PS standards with 4 μm and 5 μm were analysed and the particle size-method by Pace *et al.*[24] was used to estimate the transport efficiency. Here, the C signal of a known MP particle allows to determine the C-mass response, which can subsequently be compared to the ionic C response. Due to aerosol loss, the mass response for the ionic signal appears lower and the difference to the particle mass response allows to determine the aerosol transport efficiency. This transport efficiency was subsequently applied to calibrate both Cl and C SP signals. However, this approach assumes that particles do not influence the generation and dynamics of the aerosol as will be discussed later.

Results and discussion

Characterisation of secondary microplastics by Raman and SEM

The successful generation of secondary microplastics (MPs) through ultrasonication was confirmed using scanning electron microscopy coupled with energy-dispersive X-ray spectroscopy (SEM-EDX) and Raman microspectroscopy. SEM images and light microscope images revealed irregularly shaped fragments consistent with the physical breakdown of bulk plastics into smaller particles (see Fig. 1). EDX analysis provided elemental composition data, which confirmed the generation of MPs from both polymers PS and PVC based on the sole detection of C or its coincidence with Cl, respectively. To further validate the presence and identity of both plastic types, Raman microspectroscopy was employed. The Raman analysis confirmed the formation of secondary MPs for both PS and PVC by comparing the obtained spectra to reference spectra in the database (Fig. 1). For PS, prominent peaks were observed at 1002 cm^{-1} and 1032 cm^{-1}, corresponding to ring breathing mode and C–H in-plane deformation, respectively. PVC showed signature peaks at 638 cm^{-1} and 697 cm^{-1}, corresponding to stretching vibrations of C–Cl bonds in the fingerprint region. Slight differences between the spectra of the aged PS and PVC particles and the reference spectra were noted, which can be attributed to chemical and physical changes occurring during the aging process. These include oxidation, chain scission, and the formation of new functional groups, as well as possible leaching of additives and surface morphology changes.[25,26]

Despite the controlled laboratory experiment, unknown particles and soot were observed for both PS and PVC batches (Fig. 1). This may be attributed to localised degradation of the polymer surfaces during extended ultrasonication, or to minor contamination from the sonication bath or laboratory environment. This was relevant as it underpinned the requirement for increased selectivity when conducting light and electron microscopy and therefore, Raman and EDX modules were required to identify target MP particles for mean size estimations. The mean particle sizes (maximum diameter for non-spherical particles) were 3.6. ± 1.6 μm and 3.3 ± 2.0 μm for PS, and 3.4 ± 1.5 μm and 2.6 ± 1.7 μm for PVC using Raman microscopy and SEM-EDX, respectively. The relatively large standard deviation was attributed to the polydispersity and deviations in the aspect ratios across found particles.

Low mass analysis in SP ICP-TOFMS

Low-mass ions such as $^{12}C^+$ are strongly affected by the low-mass cut-off inherent to RF multipole ion guides. These guides impose a finite m/z transmission window with both low- or high-mass cut-offs and consequently, ions are transmitted efficiently within a certain mass range.[16] In practice, lowering the RF amplitude to improve transmission of $^{12}C^+$ simultaneously reduces transmission efficiency at higher m/z. This trade-off must be managed when detecting carbon from MPs together with heteroatoms (*e.g.*, Cl) or metals. In the here employed SP ICP-TOFMS instrument, the collision/reaction cell (CRC) was a segmented multipole;[27] accordingly, the CRC RF amplitude was tuned to balance transmission of $^{12}C^+$ and $^{35}ClH_2^+$. For optimisation, the RF amplitude was varied while acquiring spectra from m/z 7 to 40, and performance was evaluated *via* a signal-to-noise ratio (SNR) defined as the ratio of the mean single particle peak height to the compound-Poisson detection threshold ($\alpha = 10^{-6}$). The latter is frequently used to

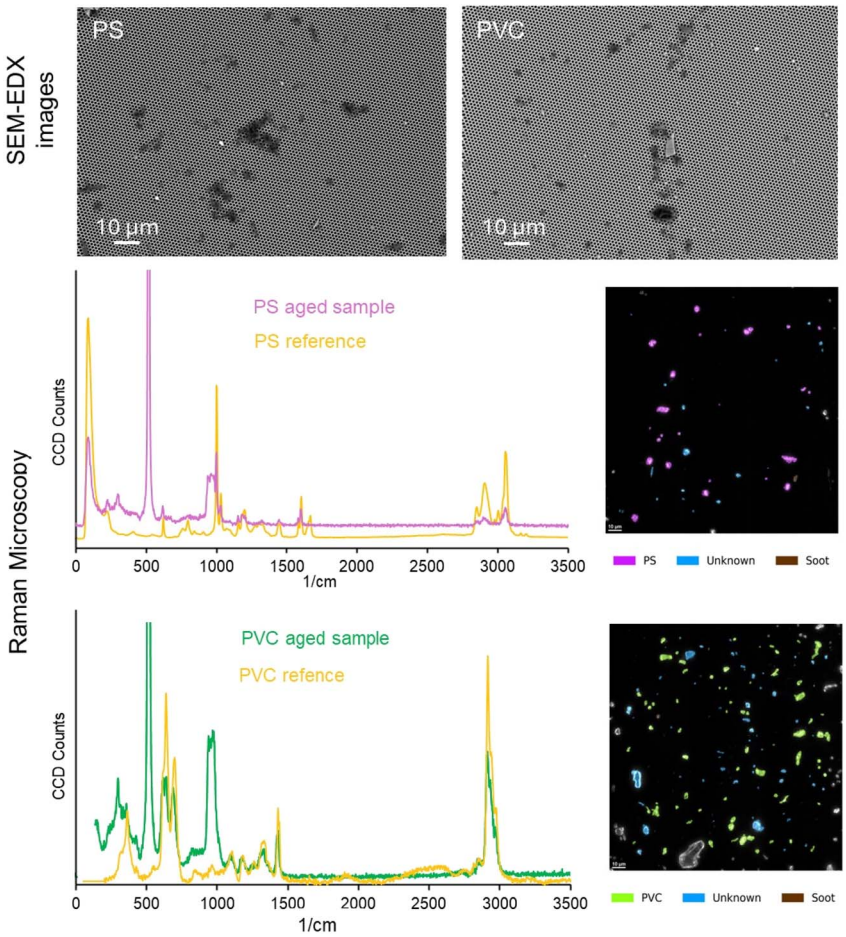

Fig. 1 Spectra and images recorded *via* SEM-EDX (top) and Raman microspectroscopy (bottom) of aged MPs generated from bulk PS and PVC are shown. The very strong band at 520 cm^{-1} and broad band around 940 cm^{-1} are attributed to the signals of the Si-filter.

differentiate random noise and SP events and was used as a noise-proxy. As a first step, parameters were optimised for carbon alone: Fig. 2A shows SP events for $^{12}C^+$, and Fig. 2B shows the dependence of both absolute SP signal and SNR on the RF amplitude. Here, the mean SP signal and signal-to-detection threshold value are shown in orange and turquoise while altering the RF amplitude from 0.3 to 0.8 V. The optimal range for SP detection of $^{12}C^+$ was found to be between 0.40 and 0.50 V.

Cl detection by SP ICP-TOFMS

Chlorine analysis by ICP-TOFMS is inherently challenging due to its high ionisation potential, strong reactivity, and spectral interferences. To overcome these limitations, we employed hydrogen as a reaction gas to promote the formation of molecular ions, specifically $^{35}ClH_2^+$ and $^{37}ClH_2^+$. This mass-shifted detection approach improved signal-to-noise ratios and enabled more sensitive and less interfered analysis of Cl in single particle events. Due to naturally high background levels of ^{39}K, targeting $^{35}Cl^1H_2^+$ was preferable over $^{37}Cl^1H_2^+$.To maximize the efficiency of this reaction, the CRC settings were optimised systematically. Hydrogen and helium flow rates were varied between 2 and 18 ml min^{-1}. Highest signals were achieved with 2 ml min^{-1} of He and 5 ml min^{-1} of H_2. To confirm and optimise the formation of these molecular ions, the isotopic ratio of the shifted peaks was examined by analysing an ionic Cl standard in ultra-pure water. The natural isotopic ratio of ^{35}Cl to ^{37}Cl is approximately 3 : 1 and following optimisation, this ratio was maintained when mass-shifting Cl signals with H_2, indicating a quantitative reaction with negligible residual $^{35}Cl^+$ and $^{37}Cl^+$.

To find a balance for the joint analysis of C and Cl within the same single event, RF settings were investigated whilst considering both elements. In this case, the aim was to find a setting, in which the limits of analysis were somewhat comparable for both $^{12}C^+$ and $^{35}Cl^1H_2^+$ to achieve a co-incidental detection in the same SP event (see Fig. 3). The optimal range for C detection was between 0.4 and 0.5 V and beyond this range, the C transmission declined sharply. In contrast and as seen in Fig. 3, the $^{35}Cl^1H_2^+$ response exhibited a steady increase with higher RF values. However, comparable size-based detection limits for both element signals could be reached at 0.5 V, which avoided a significant loss in the C signals when targeting Cl additionally. However, in cases where Cl is investigated alone or in association with heaver elements, higher RF voltages would be

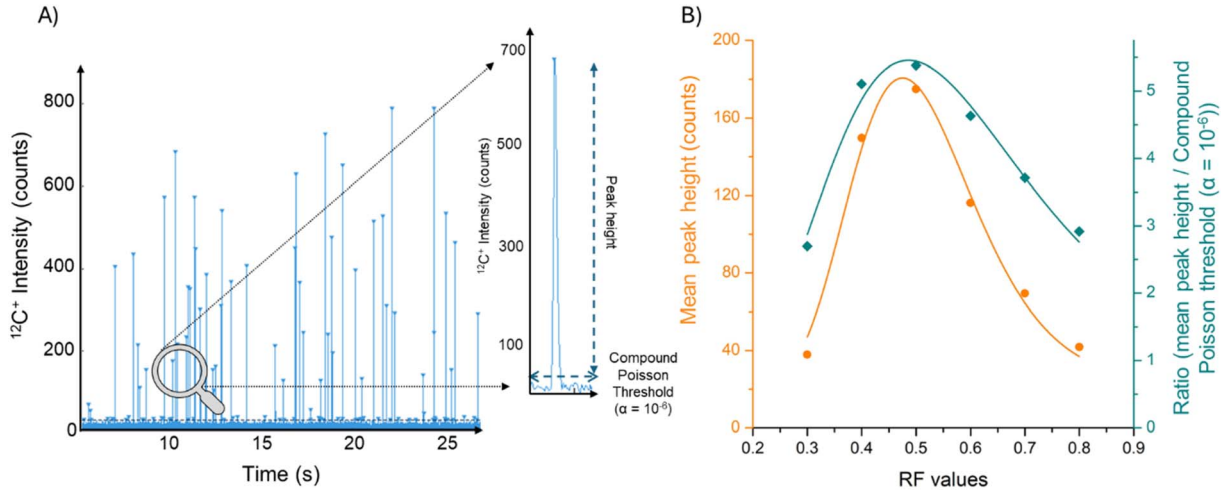

Fig. 2 Influence of RF values on $^{12}C^+$-based MP detection using a 4 μm PS standard: (A) SP event detection, including a zoomed-in view of one individual SP event. (B) Impact of RF set values on $^{12}C^+$ SP signal and signal-to-noise ratios. The signal-to-noise ratio was taken as the SP signal over the compound Poisson detection threshold ($\alpha = 10^{-6}$).

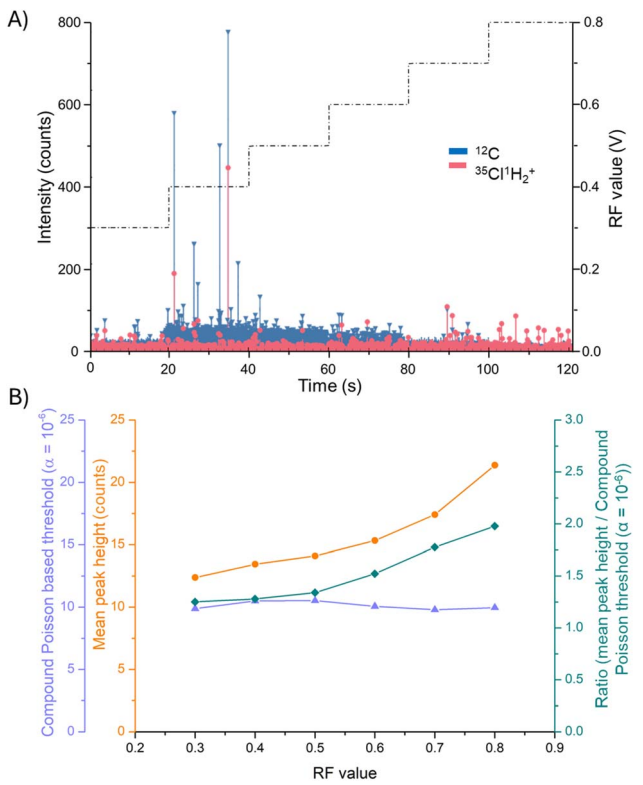

Fig. 3 Influence of RF values on the simultaneous detection of C and Cl in a PVC MP sample: (A) SP event detection of PVC MPs based on the analysis of the $^{35}Cl^1H_2^+$ and $^{12}C^+$ signals. The RF value was modified to find a range in which both signals reach similar signal to noise ratios. (B) The signal and compound Poisson threshold for the $^{35}Cl^1H_2^+$ SP signal are shown for different RF values. Their ratios were interrogated as signal to noise ratio.

beneficial. When analysing C and Cl at the same time, best achievable critical size values for PVC were 1.4 and 1.3 μm, respectively. In a recent study, Fazzolari *et al.*,[7] employed a different method using "on-mass" analysis, albeit with a different system, finding a critical size value of 3.9 μm based on the $^{35}Cl^+$ signal. Analysing Cl according to the here detailed method improved the detection limits significantly. In the future, further improvements in the detection of small PVC MPs may be achieved by accumulation of the $^{35}Cl^1H_2^+$ and the $^{37}ClH_2^+$ signals,[22] although the absence of K needs to be ensured. However, it is worth noting that SP ICP-TOFMS is determining particle mass, which is a more accurate parameter to consider, especially in cases where non-spherical particles are observed, which was the case here (compare visual analysis in Fig. 1). Here, critical mass values for C and Cl, based on total element mass within a particle, were 0.8 and 0.9 pg, respectively.

Limitations of SP ICP-TOFMS

While the critical thresholds for the detection of small particles are governed by the sensitivity and background for $^{12}C^+$ and $^{35}ClH_2^+$, the upper analysable size is constrained by transport efficiency, which decreases as particle size increases in the micrometre range. Fazzolari *et al.*[7] reported maximum analysable sizes of ~20 μm using a falling-tube device with a vertically downward-pointing torch, and ~10 μm for a conventional set-up. Using a conventional set-up, we likewise observed that particles >10 μm were rarely transported into the plasma and that transport efficiency was strongly size-dependent across the micrometre range. This was relevant here for two reasons. First, Raman microscopy and SEM-EDX indicated that approx. 12% of particles exceeded 10 μm. Second, SP ICP-TOFMS preferentially detects smaller over larger particles, biasing mass/size distributions toward lower values and preventing unbiased number-concentration estimates.

Transport efficiency in this work was determined following the size-based approach of Pace *et al.*,[24] comparing ionic-solution responses with polystyrene (PS) particle standards

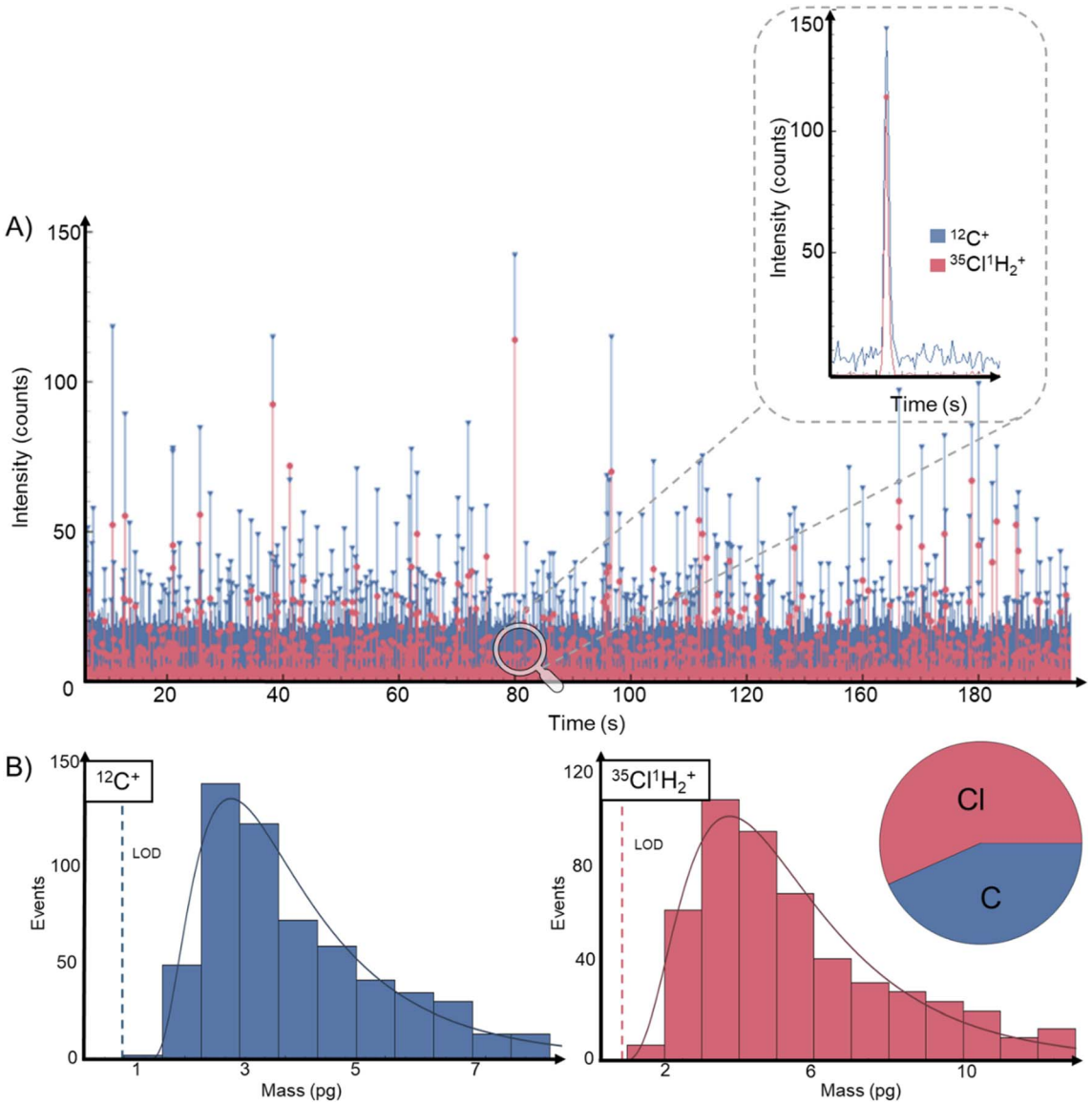

Fig. 4 (A) Transient raw data for the analysis of a PVC MP suspension. The signals $^{12}C^+$ and $^{35}Cl^1H_2$ were monitored. A magnification for one selected SP event is provided on the top demonstrating the simultaneous detection of both Cl and C within the same particle. (B) shows mass distributions of detectable MPs containing both C and Cl and a pie chart showing the mass composition of the detected PVC particles.

with known C mass, under idealised assumptions that particles do not perturb aerosol generation or transport. For increasingly large microparticles, these assumptions do not hold,[29] which limits population-level inferences: (i) although detected particles can be calibrated for particulate elemental mass, extrapolating to a true population mean mass is unreliable; and (ii) particle events can be enumerated, but size-dependent under-transport of larger MPs precludes robust particle number concentration calibration. Nevertheless, informative qualitative analyses are feasible. For example, tracking shifts in particle mass/size during degradation,[13] or distinguishing MP species within the analysable size range based on their elemental signatures.

Finally, microscopy confirmed that many MPs were non-spherical. Because conversion of particulate elemental mass to size in SP ICP-TOFMS assumes spherical geometry and a defined polymer density (yielding an equivalent spherical diameter), reported diameters should be regarded as approximate and elemental mass is preferrable as robust descriptor.

For these reasons, we report histograms and mean values for the detected fraction ("detectable particles") of MPs and provide size-based data tentatively for comparison with prior work, while emphasising that particulate elemental masses represent the more reliable metric.

Characterisation of secondary MPs by SP ICP-TOFMS

The analysis of individually aged PS-derived MPs identified detectable particles with a mean equivalent spherical diameter (ESD) of 2.2 ± 0.4 μm and a mean mass of 5.2 ± 3.7 pg (total elemental mass). For individually aged secondary PVC particles,

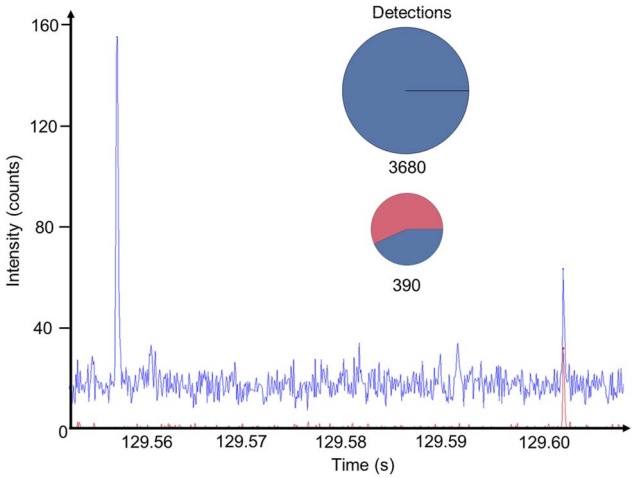

Fig. 5 Analysis of a mixture containing both aged PS and PVC MPs. PS and PVC were identified using an automated clustering, in which MP signals showing only a $^{12}C^+$ signal were identified as PS and MP events containing both $^{12}C^+$ and $^{35}Cl^1H_2^+$ signals were identified as PVC.

both C and Cl channels were used (Fig. 4). Fig. 4A shows transient $^{12}C^+$ and $^{35}ClH_2^+$ signals; the magnified event demonstrates that co-detection within a single SP event was possible enabling differentiation of polymer types by elemental composition. Size and mass distributions of detectable PVC particles yielded mean ESDs and masses of 2.4 ± 0.5 μm and 4.3 ± 2.4 pg (C-based) and 2.4 ± 0.4 μm and 6.0 ± 3.8 pg (Cl-based). Fig. 4B shows mass distributions of particle events containing a signal of C and Cl. The critical mass detection thresholds for PVC were ~0.8 pg (*via* C) and ~0.9 pg (*via* Cl), expressed as total elemental mass. For validation, we compared the Cl/C mass ratio of individual PVC particles considering the monomer sum formula C_2H_3Cl and the expected PVC mass fractions were 0.60 (Cl) and 0.40 (C). The experimental mean mass fractions were determined to be 0.57 (Cl) and 0.43 (C) and seemed to overestimate the C content slightly but within expected experimental variability.

Fig. 5 demonstrates differentiation of polymer species by hierarchical agglomerative clustering.[15,28] In a mixed sample of aged PS and PVC, detected particles were assigned to clusters based on C-only (PS) or C + Cl (PVC) signatures (distance threshold 3%, minimum cluster size 5%). For PS, the mean ESD of detectable particles was 2.2 ± 0.4 μm with a mean mass of 5.0 ± 3.7 pg (total elemental mass). For PVC, mean ESDs were 2.5 ± 0.5 μm (C-based) and 2.3 ± 0.5 μm (Cl-based) with mean masses of 5.2 ± 4.1 pg and 5.9 ± 4.9 pg based on total element mass of C and Cl, respectively. More PS than PVC particles were detected, which may reflect faster fragmentation of PS. Microscopy also revealed a small fraction (15% (PS batch) and 5% (PVC batch)) of other C-bearing particles of comparable size, which was not identified as PS or PVC; these could contribute to the C-only cluster and should be considered when interpreting PS counts.

The multi-element, single event capability of SP ICP-TOFMS enabled the assignment of particles to polymer classes and supports analysis of internal mixing (element co-location within single MPs) and external mixing (polymer-type distributions in suspensions). However, further work to parameterise transport efficiency *versus* size is required to enable robust suspension-level quantification.

Conclusions

This study demonstrates an SP ICP-TOFMS workflow that enables co-detection of carbon and chlorine within single particle events using hydrogen-assisted formation of $^{35}ClH_2^+$ and RF optimisation of the CRC to balance low *m*/*z* transmission. Using PS and PVC MPs for a proof-of-concept, particles were distinguished by elemental signatures (C-only for PS; C + Cl for PVC) and assigned by clustering. Under the presented set-up, critical detection thresholds were ~0.8 pg C (≈1.2 μm ESD) for PS and ~0.8 pg C (≈1.4 μm ESD) or ~0.9 pg Cl (≈1.3 μm ESD) for PVC. The effective analysable size range was limited by transport to roughly 1–10 μm; larger MPs were seen by Raman/SEM-EDX but rarely reached the plasma.

At present, SP ICP-TOFMS is limited to describing only a fraction of the MP population within a restricted size window, with inherent biases against larger particles. Future work should therefore focus on expanding the analysable range and on dedicated parameterisation of transport efficiency. This requires experimental set-ups that enable size-resolved transport determination and realistic correction for size-dependent losses. Moreover, the effects of particle density and shape on transport may need to be systematically evaluated.

Conflicts of interest

The authors declare no conflicts of interest.

Data availability

All data supporting the findings of this study are available within the article.

Acknowledgements

This project has received funding from the European Research Council (ERC) under the European Union's Horizon Europe research and innovation programme (grant agreement No. 101165171, project acronym: NanoArchive). Parts of the study were further supported by the FFG projects "plastic particles" (58788494, grant holder: DC). The authors further acknowledge the financial support by the University of Graz as well as by the Société des Produits Nestlé.

References

1 H. Dong, X. Wang, X. Niu, J. Zeng, Y. Zhou, Z. Suona, Y. Yuan and X. Chen, Overview of analytical methods for the determination of microplastics: Current status and trends, *Trac. Trends Anal. Chem.*, 2023, **167**, 117261, DOI: **10.1016/j.trac.2023.117261**.

2 J. P. G. L. Frias and R. Nash, Microplastics: Finding a consensus on the definition, *Mar. Pollut. Bull.*, 2019, **138**, 145–147, DOI: 10.1016/j.marpolbul.2018.11.022.
3 N. Ali, M. H. Khan, M. Ali, Sidra, S. Ahmad, A. Khan, G. Nabi, F. Ali, M. Bououdina and G. Z. Kyzas, Insight into microplastics in the aquatic ecosystem: Properties, sources, threats and mitigation strategies, *Sci. Total Environ.*, 2024, **913**, 169489, DOI: 10.1016/j.scitotenv.2023.169489.
4 N. Bostan, N. Ilyas, N. Akhtar, S. Mehmood, R. U. Saman, R. Z. Sayyed, A. A. Shatid, M. Y. Alfaifi, S. E. I. Elbehairi and S. Pandiaraj, Toxicity assessment of microplastic (MPs); a threat to the ecosystem, *Environ. Res.*, 2023, **234**, 116523, DOI: 10.1016/j.envres.2023.116523.
5 N. P. Ivleva, Chemical Analysis of Microplastics and Nanoplastics: Challenges, Advanced Methods, and Perspectives, *Chem. Rev.*, 2021, **121**, 11886–11936, DOI: 10.1021/acs.chemrev.1c00178.
6 Z. Huang, B. Hu and H. Wang, Analytical methods for microplastics in the environment: a review, *Environ. Chem. Lett.*, 2023, **21**, 383–401, DOI: 10.1007/s10311-022-01525-7.
7 S. Fazzolari, B. Hattendorf and D. Günther, Quantitative sizing of microplastics up to 20 μm using ICP-TOFMS, *J. Anal. At. Spectrom.*, 2025, **40**, 276–285, DOI: 10.1039/d4ja00323c.
8 E. Bolea-Fernandez, A. Rua-Ibarz, M. Velimirovic, K. Tirez and F. Vanhaecke, Detection of microplastics using inductively coupled plasma-mass spectrometry (ICP-MS) operated in single-event mode, *J. Anal. At. Spectrom.*, 2020, **35**, 455–460, DOI: 10.1039/c9ja00379g.
9 C. Trujillo, J. Pérez-Arantegui, R. Lobinski and F. Laborda, Improving the Detectability of Microplastics in River Waters by Single Particle Inductively Coupled Plasma Mass Spectrometry, *Nanomaterials*, 2023, **13**, 1582, DOI: 10.3390/nano13101582.
10 R. Gonzalez de Vega, S. Goyen, T. E. Lockwood, P. A. Doble, E. F. Camp and D. Clases, Characterisation of microplastics and unicellular algae in seawater by targeting carbon via single particle and single cell ICP-MS, *Anal. Chim. Acta*, 2021, **1174**, 338737, DOI: 10.1016/j.aca.2021.338737.
11 F. Gelman, M. Muszynska, J. Karasinski, O. Lev and L. Halicz, Detection of PTFE microparticles by ICP-qMS operated in single-particle mode, *J. Anal. At. Spectrom.*, 2022, **37**, 2282–2285, DOI: 10.1039/d2ja00215a.
12 R. Gonzalez de Vega, T. T. Moro, B. Grüner, T. de Andrade Maranhão, M. J. Huber, N. P. Ivleva, E. Skrzypek, J. Feldmann and D. Clases, Studying the degradation of bulk PTFE into microparticles via SP ICP-MS: a systematically developed method for the detection of F-containing particles, *J. Anal. At. Spectrom.*, 2024, **39**, 2030–2037, DOI: 10.1039/D4JA00101J.
13 M. Wieland, S. P. Schwaminger, M. Elinkmann, P. Stüger, J. Feldmann, D. Clases and R. Gonzalez de Vega, Ozone-Mediated Breakdown of Microplastics in Aqueous Environments, *J. Anal. At. Spectrom.*, 2025, DOI: 10.1039/D5JA00226E.
14 R. Gonzalez de Vega, T. E. Lockwood, L. Paton, L. Schlatt and D. Clases, Non-target analysis and characterisation of nanoparticles in spirits via single particle ICP-TOF-MS, *J. Anal. At. Spectrom.*, 2023, **38**, 2656–2663, DOI: 10.1039/d3ja00253e.
15 T. E. Lockwood, L. Schlatt and D. Clases, SPCal – an open source, easy-to-use processing platform for ICP-TOFMS-based single event data, *J. Anal. At. Spectrom.*, 2025, **40**, 130–136, DOI: 10.1039/D4JA00241E.
16 L. Hendriks and D. M. Mitrano, Direct Measurement of Microplastics by Carbon Detection via Single Particle ICP-TOFMS in Complex Aqueous Suspensions, *Environ. Sci. Technol.*, 2023, **57**, 7263–7272, DOI: 10.1021/acs.est.3c01192.
17 T. Vonderach, A. Gundlach-Graham and D. Günther, Determination of carbon in microplastics and single cells by total consumption microdroplet ICP-TOFMS, *Anal. Bioanal. Chem.*, 2024, **416**, 2773–2781, DOI: 10.1007/s00216-023-05064-0.
18 C. Neuper, M. Šimić, T. E. Lockwood, R. Gonzalez de Vega, U. Hohenester, H. Fitzek, L. Schlatt, C. Hill and D. Clases, Optofluidic Force Induction Meets Raman Spectroscopy and Inductively Coupled Plasma-Mass Spectrometry: A New Hyphenated Technique for Comprehensive and Complementary Characterizations of Single Particles, *Anal. Chem.*, 2024, **96**, 8291–8299, DOI: 10.1021/acs.analchem.3c04657.
19 E. von der Esch, M. Lanzinger, A. J. Kohles, C. Schwaferts, J. Weisser, T. Hofmann, K. Glas, M. Elsner and N. P. Ivleva, Simple Generation of Suspensible Secondary Microplastic Reference Particles via Ultrasound Treatment, *Front. Chem.*, 2020, **8**, 169, DOI: 10.3389/fchem.2020.00169.
20 S. Wolff, F. Weber, J. Kerpen, M. Winklhofer, M. Engelhart and L. Barkmann, Elimination of microplastics by downstream sand filters in wastewater treatment, *Water*, 2021, **13**, 33, DOI: 10.3390/w13010033.
21 O. Jacob, A. Ramírez-Piñero, M. Elsner and N. P. Ivleva, TUM-ParticleTyper 2: automated quantitative analysis of (microplastic) particles and fibers down to 1 μ m by Raman microspectroscopy, *Anal. Bioanal. Chem.*, 2023, **415**, 2947–2961, DOI: 10.1007/s00216-023-04712-9.
22 T. E. Lockwood, R. Gonzalez de Vega, Z. Du, L. Schlatt, X. Xu and D. Clases, Strategies to enhance figures of merit in ICP-ToF-MS, *J. Anal. At. Spectrom.*, 2023, **39**, 227–234, DOI: 10.1039/d3ja00288h.
23 T. E. Lockwood, R. Gonzalez De Vega and D. Clases, An interactive Python-based data processing platform for single particle and single cell ICP-MS, *J. Anal. At. Spectrom.*, 2021, **36**, 2536–2544, DOI: 10.1039/d1ja00297j.
24 H. E. Pace, N. J. Rogers, C. Jarolimek, V. A. Coleman, C. P. Higgins and J. F. Ranville, Determining transport efficiency for the purpose of counting and sizing nanoparticles via single particle inductively coupled plasma mass spectrometry, *Anal. Chem.*, 2011, **83**, 9361–9369, DOI: 10.1021/ac201952t.
25 X. Yu, B. Wang, C. Han, L. Liu, X. Han, B. Zheng, B. Zhang, J. Sun, Z. Zhang, W. Ma, L. Zhai and X. Lu, Physicochemical and biological changes on naturally aged microplastic surfaces in real environments over 10 months, *Environ.*

Pollut., 2023, **337**, 122522, DOI: **10.1016/j.envpol.2023.122522**.

26 A. I. Al-Mosawi and S. A. Abdulsada, Effect of aging on Raman spectroscopy analyses for flexible polyvinyl chloride, *Vib. Spectrosc.*, 2025, **138**, 103805, DOI: **10.1016/j.vibspec.2025.103805**.

27 M. Burger, L. Hendriks, J. Kaeslin, A. Gundlach-Graham, B. Hattendorf and D. Günther, Characterization of inductively coupled plasma time-of-flight mass spectrometry in combination with collision/reaction cell technology-insights from highly time-resolved measurements, *J. Anal. At. Spectrom.*, 2019, **34**, 135–146, DOI: **10.1039/c8ja00275d**.

28 M. Tharaud, L. Schlatt, P. Shaw and M. F. Benedetti, Nanoparticle identification using single particle ICP-ToF-MS acquisition coupled to cluster analysis. From engineered to natural nanoparticles, *J. Anal. At. Spectrom.*, 2022, **37**, 2042–2052, DOI: **10.1039/d2ja00116k**.

29 M. Lomax-Vogt, L. M. Carter, J. Wielinski, S. Kutuzov, G. V. Lowry, R. Sullivan, P. Gabrielli and J. W. Olesik, Challenges in Measuring Nanoparticles and Microparticles by Single Particle ICP-QMS and ICP-TOFMS: Size-Dependent Transport Efficiency and Limited Linear Dynamic Range, *J. Anal. At. Spectrom.*, 2025, **40**(3), 848–859, DOI: **10.1039/D4JA00425F**.